PAPER

Check for updates

Why do Si quantum dots with stronger fast emission have lower external photoluminescence quantum yield?†

Tomáš Popelář, [ID] [a] Filip Matějka, [ID] [ab] Jakub Kopenec, [ID] [a] Giacomo Morselli, [ID] [c] Paola Ceroni [ID] [c] and Kateřina Kůsová [ID] *[a]

Silicon quantum dots (QDs) are a promising non-toxic alternative to the already well-developed platform of light-emitting semiconductor QDs based on III–V and II–VI materials. Oxidized SiQDs or those surface-terminated with long alkyl chains typically feature long-lived orange-red photoluminescence originating in quantum-confined core states. However, sometimes an additional short-lived PL band, whose mechanism is still highly debated, is reported. Here, we perform a detailed study of the room-temperature PL of SiQDs using samples covering three main fabrication techniques. We find evidence for the presence of only one set of radiative processes in addition to the typical long-lived PL. Moreover, we experimentally determine the ratio between the short- and long-lived PL component, obtaining a wide range of values (0.003 − 0.1) depending on the type of sample. In accordance with an already published report, we observe a tendency of SiQDs with stronger short-lived PL to have lower external quantum yield. We explain this trend using a model of the optical performance of an ensemble of QDs with widely varying optical characteristics through a mechanism we call *selective lifetime-based quenching*.

1 Introduction

Silicon quantum dots (SiQDs) are a class of materials with a wide range of prospective applications stemming from their appealing properties, such as material abundance and favorable toxicity profile,[1–5] in connection with their ability to relatively efficiently emit light with highly variable properties.[6] The most intensely studied photoluminescence (PL) channel in these nanoparticles is the size tunable red to infrared PL emission with decay lifetimes in the range of hundreds of microseconds,[7–10] sometimes referred to as the S band. However, in addition to this long-lived PL channel, also much faster PL emission spectrally often located in the visible blue region has been observed. In some studies, tunability gap in the yellow/green visible spectral range between the typical long-lived and short-lived PL has been reported,[11–15] but observations of spectral tunability even through the yellow/green visible spectral range have also been published.[16–20]

The origin of the short-lived PL is still under intense discussion. The traditionally studied SiQDs are surface-terminated either with oxides or with long alkyl groups typically attached using the hydrosilylation reaction. In addition to these traditional SiQDs, there is a second class of SiQDs with short-lived emission. These are often fabricated by various chemical syntheses and feature a wide range of possible surface chemistries, sometimes reaching high values of PL quantum yield.[5,9,21–23] Naturally, tailored surface passivation can result in diverse mechanisms being responsible for light emission in these SiQDs. As an example, bandgap engineering by tensile strain and/or electronegativity have been proposed as mechanisms behind short-lived PL with fast radiative rates.[24–27] This diversity of mechanisms is further complicated by several recently published studies suggesting an unintentional formation of carbon or silica dots in presumably SiQD samples synthesized in the low-temperature reduction of silanes with citrates or in the oxidation of magnesium silicide with bromine.[28–31] These unintentionally produced carbon or silica dots can possibly contribute to or be solely responsible for the observed PL. A further complication is the controversial role of nitrogen, which has been suggested as a factor inducing the switch from the long-lived to the short-lived PL.[12] However, later studies proved it not to be always the case.[32,33] Thus, in chemically synthesized SiQDs or those terminated with diverse surface ligands, the mechanisms of PL need to be determined sample by sample.

Here, we focus on the former, more traditional class of SiQDs passivated by surface oxide or by long alkyl groups and their short-lived emission. In some cases, especially in colloidal

[a]Institute of Physics of the CAS, v.v.i., Cukrovarnická 10, 162 00 Prague 6, Czechia. E-mail: kusova@fzu.cz

[b]University of Chemistry and Technology, Technická 5, 166 28 Praha 6, Czechia

[c]Chemistry Department "Giacomo Ciamician", University of Bologna, Via F. Selmi 2, 40126 Bologna, Italy

† Electronic supplementary information (ESI) available. See DOI: https://doi.org/10.1039/d3na01031g

samples, a part of this emission is bound to originate in surface oxide as this PL emission can grow with storage time[9] or even after exposure to laser irradiation with high peak powers. However, the short-lived emission can accompany the long-lived one also in samples not exhibiting aging or improper storage. Oxide-related states,[34] very small SiQDs[35] or the direct recombination of hot carriers[36,37] have been proposed as possible origins of this short-lived PL. In reality, it likely comes from a combination of these processes.[33]

Even though many studies of this PL channel have been published, most of them rely only on the simplest PL characterization, the spectrum of the temporally integrated PL under continuous excitation. Such PL spectrum provides only a small number of clues which could possibly help determine the origin of PL. Therefore, here, we perform a detailed mapping of radiative channels in the PL of SiQDs over a very wide range of timescales from several nanoseconds to two milliseconds at room temperature. This mapping reveals the presence of two distinct sets of radiative channels, which can be identified with the typical long-lived and short-lived bands in the PL of SiQDs. This finding confirms the absence, or at least a very low importance, of additional radiative channels. Both long-lived and short-lived PL components are found in all the studied samples, which were chosen to represent the most important fabrication methods of SiQDs. Our approach also lets us determine the ratio of the emitted long-lived and short-lived PL, which varies in a wide range of values from 0.003 to 0.1 depending on the type of sample. We observe, in accordance with a previous publication by an independent group, that the ratio of these two radiative channels correlates with external PL quantum yield and samples exhibiting lower quantum yield values are characterized by relatively higher short-lived PL. This observation is explained by selective lifetime-based quenching, an effect where the introduction of a non-radiative PL channel selectively renders slowly emitting SiQDs dark without significantly influencing the fast PL channel.

2 Methods

2.1 Sample fabrication

We used the same set of samples as in our previous publication.[38] In brief, we used SiQDs synthesized in a noncommercial flow-through reactor with low-pressure nonthermal plasma, denoted as NTP:SiQDs. For subsequent hydrosilylation (NTP:SiQDs:C), the synthesized powder was collected directly to a dodecene-filled vial in the synthesis reactor and the vial was then placed onto a hot plate with an aluminum heating nest. The sample was purified using two centrifugation/precipitation cycles in an ethanol/hexane solvent/antisolvent pair and dispersed and kept in toluene. Next, SiQDs were synthesized by the thermal disproportionation of hydrogen silsequioxane (HSQ) and the SiQDs were subsequently HF-etched, yielding free-standing H-terminated particles. These were then alkyl-capped by hydrosilylation in the presence of 1-dodecene and initiated with diazonium salt, leading to the dodecene-capped QDs (HSQ-SiQDs:C).[39] The next two samples were prepared by electrochemical etching of B-doped p-type wafers in HF:EtOH

solution, following the "standard" and "white" conditions.[11] After etching, the on-wafer layer of SiQDs was intensely rinsed in pure ethanol EtOH and dried in air ("standard", denoted etch-SiQDs:a here) or underwent further treatment in H_2O_2 ("white", etch-SiQDs:b). The resulting SiQD layer was mechanically scrapedoff the substrate, SiQDs were aged under ambient atmosphere and then dispersed in EtOH. For the de-agglomeration procedure,[40] (etch-SiQDs:b), SiQDs were treated in a high power ultrasonic ethanoic bath (absorbed energy 100 kJ, 1 s on and 1 s off pulses). The mean diameter of etch-SiQDs was around 2.5–3 nm.

2.2 Optical characterization

The spectrally and temporally resolved signal was recorded by streak camera Hamamatsu C10627 (with best time resolution of 15 ps) after excitation by a femtosecond laser PHAROS (150 fs pulses, Light Conversion). The excitation wavelength was selected in the range of 315–450 nm by non-linear interactions in harmonics generator HiRO or optical parametric amplifier ORPHEUS, both by Light Conversion. The repetition rate was 1 kHz. The SiQD colloids were placed in quartz cuvettes and the luminescence signal was collected under a 90° angle using a set of lenses. All data were corrected for the spectral sensitivity of the whole setup by multiplying the spectral profiles deduced from the analysis described below with the corresponding correction curve.[41] All measurements were carried out at room temperature.

The PL decay measurements were made as a function of wavelength and were transformed into emission photon energies in eVs including the $1/\lambda^2$ spectral correction factor.[42] Using a method described earlier,[38,41] we took into account also the onset of PL in the PL decay curves, which results in much more accurate fits. The emission-photon-energy dependent series of PL decays $I(\lambda, t)$ was thus fitted using a convolution of a Gaussian curve and a fitting function. The Gaussian curve represents the laser pulse as measured by the detection system, or the instrumental response function. Its characteristics are known and fixed in the fit because they had been determined prior to the measurement of PL. The PL decay function is assumed to be stretched-exponential[38] $I = I_0 \exp\left\{-\left(\dfrac{t}{\tau_{SE}}\right)^\beta\right\}$ unless stated otherwise. Thus, a set of λ-dependent PL decay parameters ($\tau_{SE}(\lambda)$ and $\beta(\lambda)$) and the spectral profile $I_0(\lambda)$ were obtained from one PL map. The normalization of the decay function (*e.g.* the stretched-exponential) at each λ to unity ensures that the value of $I_0(\lambda)$ corresponds to the integrated PL intensity at the particular λ. Thus, $I_0(\lambda)$ represents the spectrum of the corresponding PL component. Instead of the stretched-exponential lifetime τ_{SE}, the more physically meaningful average PL lifetimes $\tau_{av} = \dfrac{\Gamma\left(\dfrac{2}{\beta}\right)}{\Gamma\left(\dfrac{1}{\beta}\right)}\tau_{SE}$ are reported.[38]

The longer-timescale PL decays in Fig. 2a and b with a 500 and 100 μs temporal window were fitted using the typical stretched-exponential function. The characterization of shorter-

timescale temporal windows of 1 μs and 100 ns was more problematic because only the initial part of the decay of the slow component is present, which in general can lead to improperly determined lifetimes.[41] Thus, in order to properly characterize the 1 μs temporal window (Fig. 2c), the PL decay parameters τ_{SE} and β of the long-lived component were fixed at values obtained in the longer temporal windows and only the amplitude (spectral profile) of the long-lived PL component was treated as a free parameter. The fast component was described by a stretched-exponential function and iterative steps of fixing some of the parameters and fitting were performed to obtain a good fit.[41] An analogical approach was used for the fitting of the 1 μs PL decays in Fig. 4. The corresponding spectral profiles were then extrapolated as a Gaussian and pseudo-Voigt profile for the long-lived and the short-lived component, respectively, and spectrally integrated to yield the overall PL intensity emitted in the two components. Once again, the spectral position of the PL maximum is known from the measurements using other temporal windows (1 ms or 500 μs for the long-lived, and 20 or 50 ns for the short-lived component, respectively) and, therefore, only the amplitude (PL intensity) and possibly the width of the peak are kept as a free fitting parameter when extrapolating the spectral profiles. The Gaussian function fits the spectral profile of the long-lived component perfectly. The pseudo-Voigt function is not a perfect approximation of the spectral profile of the short-lived PL component, however, given the order-of-magnitude differences in the fast-to-slow ratio of the studied samples, the error resulting from this approximation is negligible for the purposes of this study.

The QYs were measured by the absolute method (integrating sphere setup) following the procedure in ref. 43 where the LEDs were replaced by the laser-driven light source (EQ-99X, Energetiq) coupled to the 15 cm monochromator (Acton SP 2150i, Princeton Instruments) as the excitation source.

3 Results and discussion

3.1 Identification of PL components

In Fig. 1a and b we present the bandstructure of bulk silicon and the corresponding "fuzzy" bandstructure of SiQDs,[44] which serves as a basic model of the electronic properties of SiQDs in general. Here, we summarize the most important recombination channels in this material. The most notable source of radiative recombination are clearly (i) the direct $\Gamma_{15} - \Gamma'_{25}$ transitions in the Γ point which are likely to be fast as a result of their direct nature, and (ii) the indirect lowest-excited state Γ_{15}–X_1 transitions. Since the oscillator strength of the transition decreases as the $\vec{k}$-space overlap of the electron–hole wavefunction decreases, the latter transitions are relatively slow (≈ 100 μs) and are responsible for the classical red emission in SiQDs,[7,45,46] which we investigated in more detail in our previous article.[38] In an ideal hypothetical case, the PL measured in an SiQD sample should reflect these two radiative pathways, as sketched in the schematic image in Fig. 1c. Even though, in the case of the fast $\Gamma_{15} - \Gamma'_{25}$ channel, the observation of light emission from effectively hot states might seem counter-intuitive as competitive phonon-emitting thermalization processes are typically much faster, in SiQDs, a broad interval of phonon thermalization rates are known to exist[47] as a result of the quantization of electronic levels. Thus, in a non-negligible fraction of QDs in the ensemble,[47] the effective phonon or multi-phonon thermalization rates will be relatively slow, even reaching the nanosecond scale. The connection between the direct transition and the blue PL had already been made in the past in several reports.[33,36,37,48]

In order to test if our assumption about solely slow and fast radiative pathways in SiQDs holds, we chose a set of samples fabricated by several methods with both oxide and long-alkyl surface passivation. The samples are listed in Table 1, their
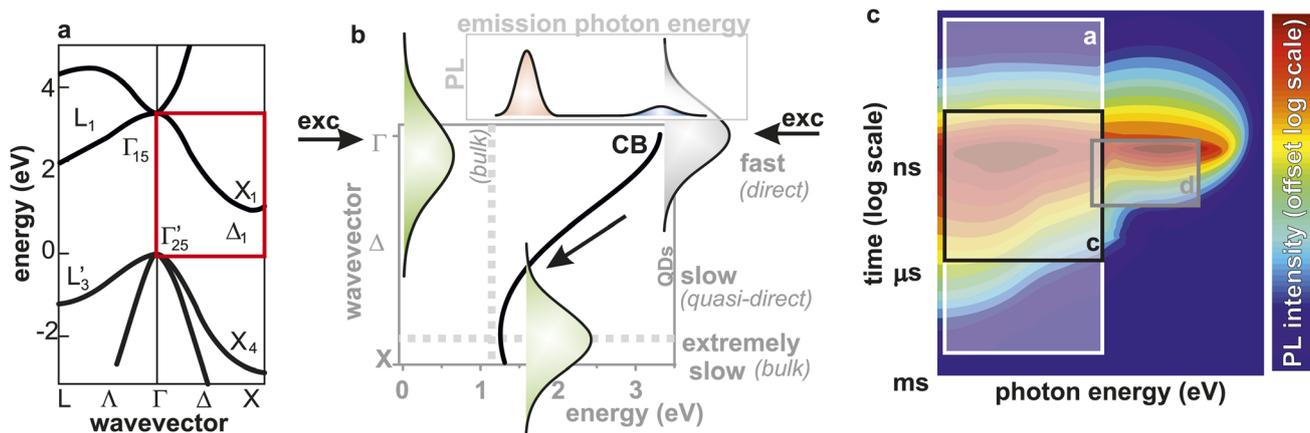

Fig. 1 Carrier relaxation in SiQDs. (a) Bandstructure of bulk silicon. (b) A 90 degree rotated cross-section of the conduction band of bulk silicon (the red rectangle in panel (a)). The electron and hole wavefunctions of the lowest excited state of an SiQD are shown by the green areas, the gray wavefunction represents the energetically lowest position possibly resulting in a direct transition and the black arrows denote relaxation after the excitation event. Larger $\vec{k}$-space overlap between the electron and hole wavefunctions correlates with faster radiative rates. Extremely slow purely indirect bulk Si radiative transitions are shown with the dotted line for comparison. The top panel plots a PL spectrum corresponding to the two expected types of radiative transitions. (c) A scheme of temporally and spectrally resolved PL from SiQDs based on the mechanism from the previous panel (please note the logarithmic scales). The highlighted areas correspond to PL measurements in Fig. 2.

Table 1 List of the studied samples and their optical properties[a]

Label	Fabrication	Surface	QY (%)	τ_{av} (ns)	β	λ_{max}^{short} (eV)	λ_{max}^{long} (eV)
NTP-SiQD:C*	Non-thermal plasma synthesis	Alkyl	6	15	0.5–0.6	2.70	1.78
HSQ-SiQD:C*	Thermal disproportionation of HSQ	Alkyl	26	≈3.5	0.65	3.12	1.73
etch-SiQD:Oa	Electrochemical etching of Si wafers	Oxide	6.8	20	0.63	2.95	1.76
etch-SiQD:Ob*	Electrochemical etching of Si wafers	Oxide**	2.3	4–5	0.55	2.54	1.96

[a] Samples marked with an asterisk (*) were shown to be fully radiative in the long-lived PL channel ($\eta_{slow} = 1$) in our previous work,[38] double asterisk (**) shows that the sample underwent a deagglomeration treatment. Photoluminescence quantum yield (QY), the characterization of the short-lived component (average lifetimes τ_{av} and dispersion parameters β) as well as the spectral position of the PL maximum for the short- and long-lived ($\lambda_{max}^{short/long}$) component, respectively, are listed. The short-lived PL component was characterized under UV excitation.

basic properties are presented in ESI.† The studied SiQDs were (i) synthesized in non-thermal plasma (NTP-SiQDs), (ii) synthesized by annealing of an Si-rich SiO_x precursor and subsequently extracted from the matrix (HSQ-SiQDs), or (iii) fabricated by a top-down approach by electrochemical etching of a monocrystalline Si wafer (etch-SiQDs).[11] The SiQD samples were then either oxidized under ambient conditions for at least a month (SiQDs:O) and dispersed in a solvent, or were surface-terminated by hydrosilylation with 1-dodecene and purified (SiQDs:C).

Using this set of samples, we performed a series of temporally and spectrally resolved PL measurements covering a wide range of timescales and photon emission energies as proposed in Fig. 1c, yielding PL "maps". These PL maps were then analyzed as a series of PL decays at different emission wavelengths, or emission photon energies λ. The result of the analysis of one PL map is thus a λ-dependent profile of the corresponding lifetimes and emission intensities. The lifetimes, in the form of the intensity averaged lifetimes τ_{av},[38] can be either λ-dependent or constant. The λ profile of the PL intensities then constitutes the spectral profile of the corresponding PL component. Thus, our analysis allowed us to separate the individual components in the PL signal and determine both their lifetimes and spectral profiles. The corresponding procedure is detailed in Section 2.2.

The process of characterizing a wide range of photon emission energies (380–1000 nm, or 1.24–3.26 eV) and timescales (1 ns–2 ms) with sufficient resolution at the same time would be an ideal tool to map all the PL processes present in the materials. Such PL "mapping" would result in an idealized schematic PL map shown in Fig. 1c. However, the PL mapping of the whole PL emission process as sketched in Fig. 1c is technically not simple due to various complications, such as the possibility of a second-order signal of the spectrograph grating in a wide spectral window or the limited dynamic temporal range of the detector which makes it impossible to simultaneously characterize nanosecond and microsecond processes with sufficient temporal resolution. Therefore, we used several measurements with different settings (emission photon energy, the timescale) to cover the idealized PL map from Fig. 1c. Examples of these different measurements presented in Fig. 2 are highlighted as the translucent rectangles overlaying the PL map in Fig. 1c.

The PL signal measured in the commonly studied range of hundreds of microseconds or more (Fig. 2a) follow the typical

shape of the long-lived, slow component we investigated earlier.[38] Despite the higher noise levels in the shorter temporal windows, the PL decays still keep their typical shapes, as evidenced by the selected PL decay shown as an overlay of the PL map in Fig. 2b. At the 1 µs (Fig. 2c) temporal window, the long-lived component starts to appear very flat as only a very small initial part of the PL decay is detected.

In principle, PL decays acquired using the shorter timescales such as those in Fig. 2b and c could be simply fitted to evaluate the corresponding lifetimes and spectral profiles. However, fitting of truncated PL decays, artificially and incorrectly distorts the deduced lifetimes.[41] Therefore, to compare the PL decays measured at different timescales, we plotted the PL decays measured at different temporal windows in a single graph, see Fig. 2e. The shape of these PL decays is clearly very similar, independent of the timescale. Therefore, we used the lifetime deduced from the long-timescale measurement[38] as a fixed parameter characterizing the long-lived PL in the shorter-timescale measurements (100 µs–100 ns), which allowed us to extract the spectral profiles corresponding to the long-lived PL component when measured using a shorter-timescale temporal window. In this way, we found out that the long-lived component can be well characterized using the same λ lifetime dependence and the same spectral profile, regardless of the timescale of the measurement. These findings corroborate the existence of a single type of process on the microsecond timescale described by the same average lifetimes. Notably, the long-lived component exhibits a spectral profile very well described by a Gaussian curve.

Upon closer inspection, a relatively fast ($\ll 1$ µs) spectrally blueshifted component appears in the 1 µs and 100 ns temporal windows in Fig. 2c, d and f. To characterize it properly, an even shorter temporal window of 10 or 20 ns needs to be chosen to be able to obtain enough details of the PL decay to produce a correct characterization. Such detailed characterization of the short-lived PL in the HSQ-SiQD:C sample is presented in Fig. 3, where we also varied the excitation wavelength. Clearly, the decay shape is highly non-single-exponential and can be very reasonably described using a stretched-exponential function with relatively low dispersion parameter (typically around 0.5–0.6). The lifetimes seem to be rising towards lower emission photon energies λ (the red part of the emission spectrum), but this effect is most likely connected with the increasing importance of the long-lived component in this spectral region, see
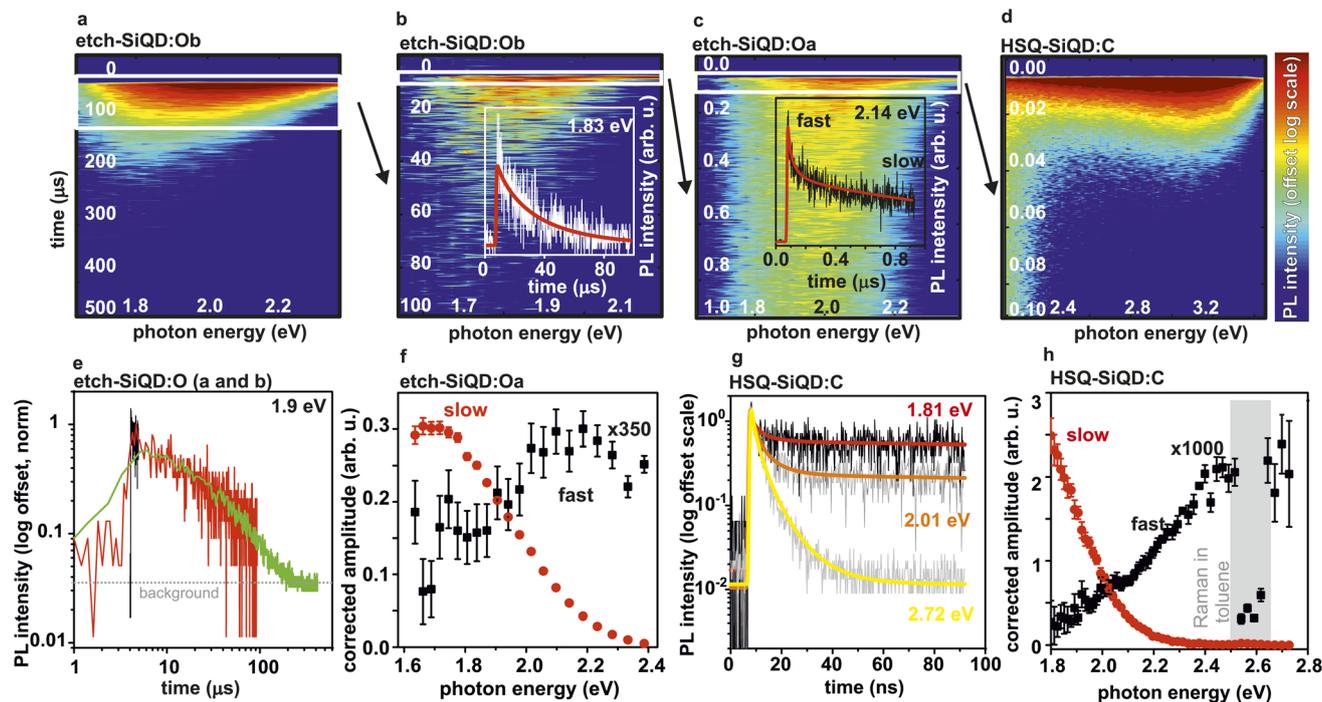
Fig. 2 Detailed characterization of PL emission in SiQDs with spectral and temporal resolution. Measurements from different samples were selected to best illustrate the main trends, the top label at each panel includes the type of sample. (a–d) Examples of measured PL maps in gradually shorter acquisition windows. In two panels, a selected cross-section is included as an overlay. White and black datapoints, respectively, are the measured data, the red curves represent the fits. (e) Direct comparison of PL decays of the long-lived component at the 1.9 eV emission photon energy from panels (a–c). (f) Spectral profiles of the long- and short-lived components obtained from the measurement in panel (c). (g) Selected PL decays from panel (d) (the black and gray datapoints) and the corresponding fits (the yellow, orange and red curves) assuming a combination of a long- and a short-lived component. Please note the clearly rising importance of the short-lived component with higher emission photon energy (or bluer emission). (h) Spectral profiles of the long- and short-lived components obtained from the measurement in panel (d).
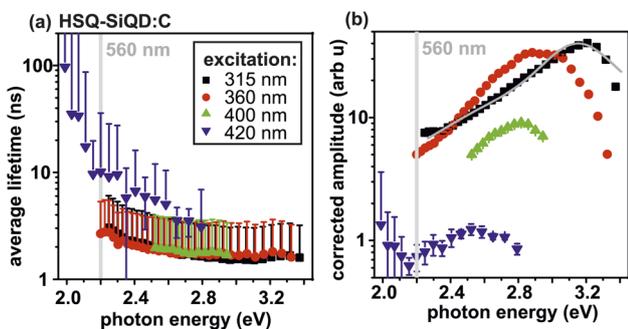

Fig. 3 The dependence of the short-lived component on the excitation wavelength under pulsed excitation obtained in a temporal window of 10 ns for sample HSQ-SiQD:C: (a) the average lifetimes, (b) the spectral profiles of the short-lived component. The black dataset of the spectral profile in panel (b) was fitted with a pseudo-Voigt profile (the gray curve).

Fig. 2f and h. The rising importance of the long-lived component is supported by the seemingly longer lifetimes characterizing the decays under the 420 nm excitation wavelength (the blue data in Fig. 3a and b) with the sharply rising tail towards lower emission photon energies. In this case, the long-lived component clearly starts to play a more and more important

role in the emission process at lower photon emission energies, it is no longer possible to mathematically separate the fast and slow processes. The average lifetimes are thus mostly λ- and excitation wavelength independent and of the order of several (3.5–20) nanoseconds, see Fig. 3a. The spectral profiles of the short-lived component have highly asymmetrical shapes with tails towards lower λ, their PL maximum redshifts with increasing excitation wavelength. The emitted short-lived PL is much stronger under UV than under blue excitation, see Fig. 3b. All these effects agree with previous reports on PL under continuous excitation.[35,37] The characterization of the short-lived PL of all the studied samples is summarized in Table 1.

The PL characteristics of the short-lived component well agree with the proposed hot-PL origin: the redshift is consistent with the size dependency of the direct $\Gamma_{15} - \Gamma'_{25}$ transition[36] and the highly non-single-exponential character of the PL decay together with the strongly asymmetric spectral profile very likely result from the radiative relaxation of unrelaxed hot carriers at the Γ point and close to it, where a competition of over-the-bandgap recombination and intraband relaxation occurs. This characteristic is in contrast to the long-lived PL originating in the first excited state, whose spectral profile is highly Gaussian, reflecting only the size-induced changes of the PL spectrum emitted by individual QDs. An additional observation

confirming the hot-electron origin of the fast channel is its decreasing intensity with shifting the excitation wavelength from UV to the blue region, as less carriers are excited over the direct bandgap. In reality, the fast channel is very likely a mixture of hot direct silicon transitions and transitions involving various surface or interface defects, with the ratio between these two being possibly sample-dependent based on the type of surface passivation and its quality. This interpretation is also supported by our previous work,[33] where we identified SiO_2-defect related and Si-core-related radiative channels in the short-lived PL using PL component analysis.

Thus, by detailed scanning of the PL characteristics from 10 ns to 2 ms, we verified that there are two dominant sets of PL processes in SiQDs as put forward in Fig. 1b and c, even though the dispersion in the corresponding values of lifetimes is relatively broad. One could argue that the asymmetry of the spectral profile of the short-lived component in Fig. 3b implies the existence of a third "intermediary" component,[36] however, we see this interpretation as improbable because of the continuous evolution of the λ dependence of average lifetimes, best documented by the average lifetimes of the short-lived component under 420 nm excitation wavelength (the blue data in Fig. 3). In addition to the well-established view of slow and fast band in SiQDs' PL,[11,49] our analysis (i) proves that only very little PL signal is present outside of these two bands, (ii) proves that the characteristic lifetimes of these two components change with the photon emission energy gradually and in a physically understandable manner.

3.2 Fast-to-slow ratio

An important question connected with the fast, short-lived component is its intensity relatively to the slow, long-lived one. Under continuous excitation, the fast and slow processes will proceed with considerably different rates. The dynamics of PL and thus the fast-to-slow ratio is governed by a set of differential equations. However, in contrast the already published description,[51,52] the short-lived component also need to be included. Such inclusion would then require explicit and accurate knowledge of the underlying radiative and nonradiative processes and their rate constants. This is a rather laborious task and it is not the goal of this work.

Thus, instead of applying continuous excitation or rigorously solving a set of differential equations with many parameters of uncertain values, we approach this problem experimentally and use low-intensity short-pulsed excitation because under low pulsed excitation most QDs are excited only once before the next excitation event occurs. If all the excited carriers are let to reach the ground state before the next excitation event, the collected signal will represent the correct ratio of the long- and short-lived components in the sample, which could be connected directly to the ratio of QDs emitting each type of PL through the respective quantum yields.

One additional complication here is that both the long-lived, "red" PL intensity and the short-lived, "blue" PL intensity should be characterized in a single measurement to avoid potential inaccuracies connected with the comparison of data measured under different experimental settings. Fortunately, such a direct comparison of the PL intensity of the two PL components is possible if an acquisition window with a suitable temporal and spectral range is selected. An ideal temporal window suitable for both the fast and slow bands is that with the range of 1 μs, as is illustrated in Fig. 2c and f for the case of the etch-SiQD:Oa sample. Actually, further measurements demonstrate that the 1 μs acquisition window allow the detection of both components in all the studied samples. Therefore, each of the studied samples were measured using the 1 μs temporal window and spectral profiles of the two PL components were deduced. Examples of one PL decay for each of the samples is shown in Fig. 4a–d. As a result of the spectral width of the acquisition window and differences in the spectral maxima of the long-lived component in each of the studied samples, the collected data cannot cover the whole spectral range of PL emission (see Fig. 1c) and need to be spectrally extrapolated in order to obtain all the PL signal emitted within both the components. Fortunately, the spectral shape of each of the components is known from a separate characterization of the long- and the short-lived component: the spectral profile of the long-lived component is highly Gaussian if plotted in emission photon energies, whereas the spectral profile of the short-lived component is highly asymmetric. A reasonable, albeit not perfect approximation of the spectral shape of the short-lived component is a pseudo-Voigt function, as is shown in Fig. 3b by the gray curve. Thus, using the knowledge of the spectral shape and the spectral position of the maximum of each of the PL bands, it is possible to make a spectral extrapolation over the necessary spectral range, as is shown in Fig. 4e for sample HSQ-SiQD:C. Using this extrapolation, it is now easy to correctly calculate the PL intensity I_{slow} and I_{fast} emitted by each of the components under sparse pulsed excitation. In this way, we can easily calculate the fast-to-slow ratio of PL intensity within each of the components

$$\text{FTS} = \frac{I_{fast}}{I_{slow}}.$$

The characterization of the four studied samples shows that the FTS ratio varies over a wide range between 0.003 and 0.1 depending on the sample. This significant difference in relative intensity might explain why the short-lived PL band is sometimes not reported on even though it was found in all the samples we study here. In some cases, the short-lived PL band might not have been found simply as a result of experimental conditions, using insufficiently sensitive detection or using excitation in the blue visible spectral range, which clearly leads to a lower intensity of the short-lived PL, see Fig. 3b.

3.3 Ensemble-averaged quantum yield in SiQDs

In the field of device design, external PL quantum efficiency typically encompasses the influence of external factors such as outcoupling of the light emitted by an LED. However, as discussed in detail by Popelář et al.,[38] in QDs, external PL quantum efficiency relates to the measured characteristics of an

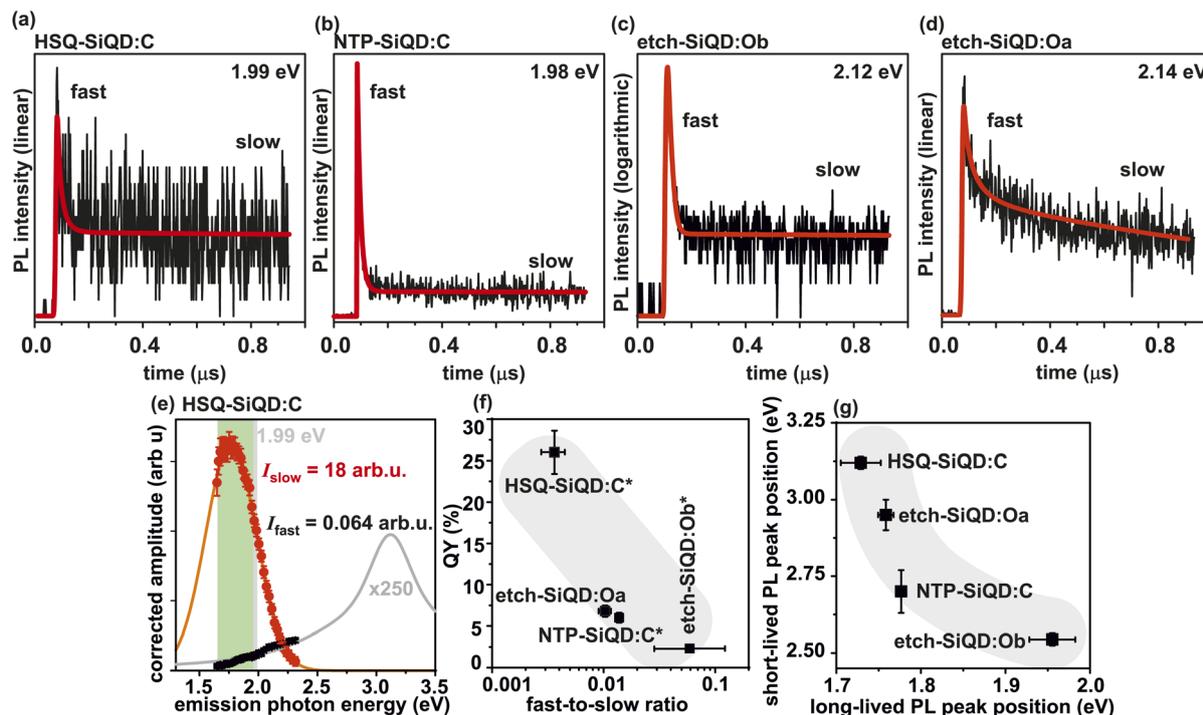

Fig. 4 (a−d) Examples of PL decays in a 1 μs window for the individual studied samples. Sample labels are noted at each panel. The black curves represent the measured data, the red curves are the fits. Please note the logarithmic vertical scale in panel (c), in which the logarithmic scale was necessary to visualize both components. To ensure that the results are comparable from one sample to another, all measurements were carried out using UV excitation (315−343 nm). (e) Spectral profiles of the long- and short-lived components deduced from the measurements shown in panel a, the spectral position of which is highlighted by the gray vertical line. The black and red datapoints show the λ dependence of the PL intensity of each of the components, the gray and orange curves are extrapolations used to estimate the overall PL intensity emitted in each of the bands. The shape of the spectra and the spectral position of each peak is known from other measurements, therefore, only the amplitude and possibly the width of the peak need to be fitted. In this sample, the PL peaks are the most far apart and, therefore, in this example, the data are extrapolated the most. The green area marks the spectral range investigated by Brown et al.[50] (f) The ratio of the PL intensity emitted in the long- and short-lived components for the samples under study, deduced using methodology from panel (e). The fast-to-slow ratio is plotted as a function of PL quantum yield. Samples with high internal quantum yield ($\eta_{slow} \approx 1$) as shown in our previous work[38] are marked with an asterisk. (g) The PL peak positions of each of the components for the samples under study. Please note how the two peaks systematically shift in opposite directions. The gray areas in panels (f) and (g) serve as guides for the eye.

ensemble, whereas internal PL quantum efficiency refers to the radiative and non-radiative processes in a "typical" QD. Clearly, finding a relation between measured quantum yield and the lifetimes of radiative and non-radiative processes becomes difficult when the ensembles of QDs are made up by sub-ensembles with significantly different optical characteristics. In that case, the relative populations of the individual sub-ensembles need to be known if any meaningful comparison is to be made. Even though this important distinction is sometimes overlooked,[53] it is especially important in slowly emitting SiQDs, where the influence of non-emitting dark SiQDs on the measured PL quantum yield is large.[38]

To simplify the problem of describing a large ensemble of QDs with significantly varied optical performance and a large number of recombination pathways, we will apply a description analogous to the experimental results presented in the previous section. Namely, we will classify the QDs into two classes of light-emitting QDs, fast and slow, and add the dark ones. As the lifetimes of the slow and fast QDs differ by several orders of magnitude, a typical lifetime can be used to describe the slow

and fast sub-ensembles of QDs, respectively, especially when their overall impact on optical performance is assessed. However, despite this typical lifetime, the existence of a distribution of lifetimes and a distribution of emission photon energies within each of the sub-ensembles is still acknowledged. In the slow recombination channel, we showed previously that the radiative lifetimes are emission-photon-energy dependent, but very similar for SiQDs fabricated by different techniques in different laboratories.[38] The characterization of the fast channel is more complex, however, the highly non-single-exponential dynamics, the differences between the lifetimes in the individual samples and the asymmetric spectral profile reported here are a phenomenological description of a competition between fast radiative, fast non-radiative and electron cooling processes. This description is summarized in Fig. 5.

In general, the internal PL quantum yield η^{QD} of a selected QD characterized by its radiative and non-radiative lifetimes $\tau_{R/NR}^{QD}$ can be calculated as
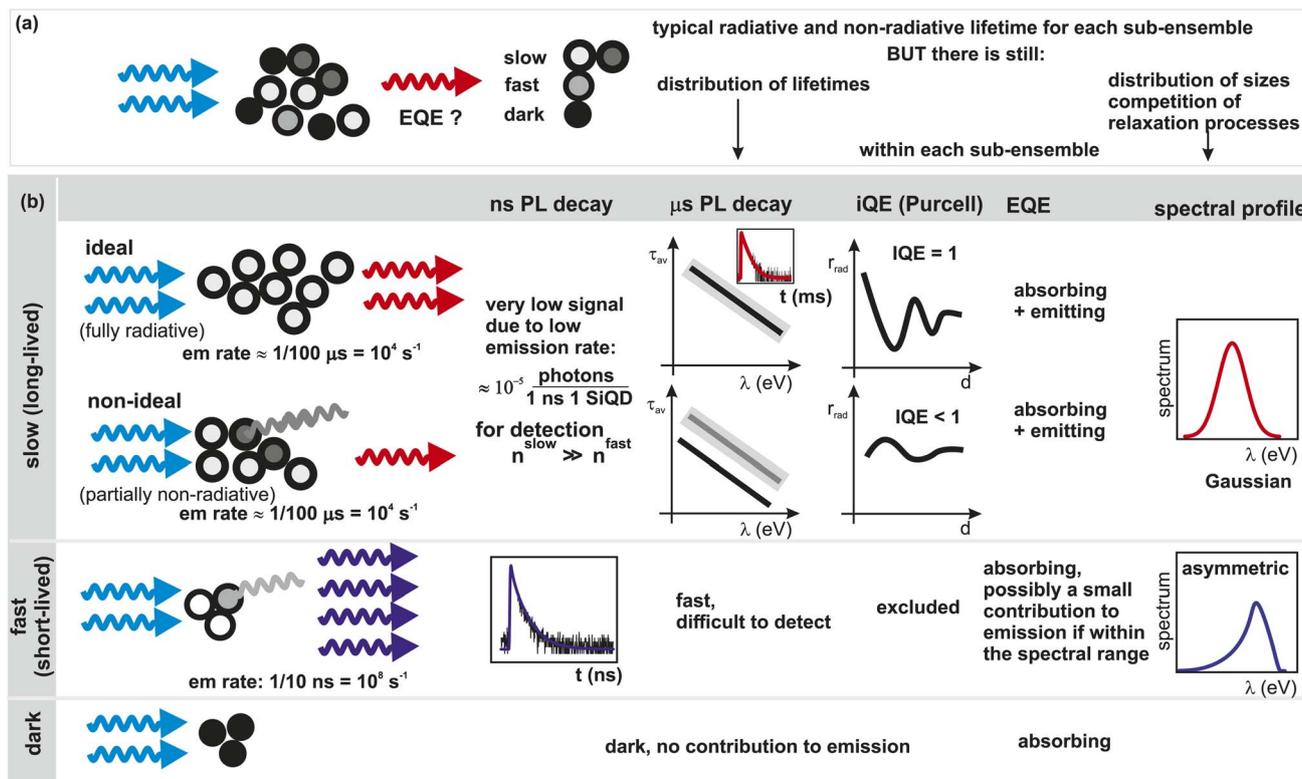
Fig. 5 (a) The basic model for the description of the optical performance of an ensemble of SiQDs. Each of the three sub-ensembles can be characterized by a typical lifetime, but a certain distribution of lifetimes and emission photon energies still exists within each sub-ensemble. (b) Typical optical properties of the three sub-ensembles. The typical red-orange radiative channel is long-lived (slow). It can be fully radiative, in which case the emission photon energy dependence of the decay lifetimes follows an exponential curve quantified by Popelář et al.[38] In some samples, slow non-radiative processes are present. The measurements of both internal and external PL quantum yield focus on this channel. Sometimes, a blueshifted short-lived (fast) radiative channel is reported on. In our samples, this channel was always detected, albeit in a very variable ratio with respect to the long-lived channel, ranging from 0.003 to 0.1. This fast channel has been observed to increase in samples with lower external quantum yield, as shown in Fig. 4f and by Pringle et al.[8] Non-emitting dark QDs influence the optical measurements only by absorbing the excitation light.

$$\eta^{QD} = \frac{\frac{1}{\tau_R^{QD}}}{\frac{1}{\tau_R^{QD}} + \frac{1}{\tau_{NR}^{QD}}} = \frac{\tau_{NR}^{QD}}{\tau_R^{QD} + \tau_{NR}^{QD}} \quad (1)$$

Moreover, the corresponding PL lifetime which would be measured if that particular QD was optically probed τ_{PL}^{QD} is the reciprocal sum of the lifetimes of the individual processes

$$\frac{1}{\tau_{PL}^{QD}} = \frac{1}{\tau_R^{QD}} + \frac{1}{\tau_{NR}^{QD}}. \quad (2)$$

Based on our experiments and the observed lifetimes, the radiative and non-radiative processes can be divided into "slow" ($\approx(1–100)$ μs) and "fast" ($\approx(1–100)$ ns). However, only certain combinations of fast/slow processes are physically relevant, as detailed in Table 2. In particular, slow non-radiative processes can be neglected in QDs with fast radiative lifetimes because their influence is minimal. Next, the combination of fast non-radiative and slow radiative processes results in extremely low internal quantum yield, rendering

such QDs dark. Therefore, looking at the ensemble macroscopically, the QDs can be categorized into three sub-ensembles, namely:

(i) slowly emitting QDs, characterized by slow radiative and non-radiative processes $\tau_{R/NR}^{slow}$,

(ii) QDs with fast emission, characterized by fast radiative and non-radiative processes $\tau_{R/NR}^{fast}$, and

(iii) dark QDs, with slow radiative lifetime and fast or extremely fast non-radiative recombination, which cannot be experimentally detected in PL.

The slowly emitting QDs can possibly also be ideal (without detectable non-radiative recombination), in that case the corresponding non-radiative recombination would be extremely slow. The internal quantum yield of a typical slow and fast QD $\eta_{slow/fast}$ can then be calculated by inserting the corresponding typical lifetimes $\tau_{R/NR}^{slow/fast}$ into eqn (1).

The measured, ensemble-averaged quantum yield η_E can be thought of as the sum of the contributions of the individual QDs. Using the description of three sub-ensembles characterized by a typical internal quantum yield $\eta_{slow/fast}$ we can write:[38]

Table 2 A list of possible combinations of slow and fast radiative and non-radiative lifetimes $\tau_{R/NR}^{QD}$ with two typical values of 100 μs and 10 ns. The values of internal PL quantum yield η^{QD} and PL lifetime τ_{PL}^{QD} are calculated based on eqn (1) and (2). The QD can then be classified as slow, fast or dark, depending on the combination of the two values. The properties of these categories of QDs are further described in Fig. 5

	$\tau_{NR}^{QD} \gg$ 100 μs (none)			$\tau_{NR}^{QD} =$ 100 μs (slow)			$\tau_{NR}^{QD} =$ 10 ns (fast)		
	τ_{PL}^{QD}	η^{QD}	Classification	τ_{PL}^{QD}	η^{QD}	Classification	τ_{PL}^{QD}	η^{QD}	Classification
$\tau_R^{QD} =$ 100 μs (slow)	100 μs	1	Slow (ideal)	50 μs	0.5	Slow (non-ideal)	10 ns	10^{-4}	Dark
$\tau_R^{QD} =$ 10 ns (fast)	10 ns	1	Fast	10 ns	1	Fast	5 ns	0.5	Fast

$$\eta_E = \frac{\sum_j n_j \eta_j^{QD}}{\sum_j n_j} \approx \frac{n^{slow}\eta_{slow} + n^{fast}\eta_{fast}}{n^{slow} + n^{fast} + n^{dark}}, \quad (3)$$

where $n^{slow/fast/dark}$ denotes the relative fraction of each of the sub-ensembles of SiQDs ($n^{slow} + n^{fast} + n^{dark} = 1$).

Based on the measurements presented in Section 3.1, we can assign the slow and fast emission to the indirect (cold electron state) and direct (hot-electron state) PL channels from Fig. 1b, respectively. In a general case, the contribution of a cold- and hot-electron state to the PL QY can be complicated, because the cold-electron state can be fed into by the depletion of the hot-electron state and the hot-electron state can be filled through Auger recombination at higher excitation intensities. These processes would necessarily affect the ratio of slow and fast PL channels. However, in our experiments presented here and in the measurements of PL QY, low excitation intensity is used to ensure the accurate determination of the corresponding physical quantities. Thus, most of the QDs are single excited and, therefore, (i) Auger recombination can be neglected and (ii) at each recombination event, each QD can be categorized as either "slow", "fast", or "dark". We do not *a priori* exclude the possibility that one QD can switch between fast and slow emission, but we deem the fraction of such QDs miniscule since they would need to have both slower thermalisation (to allow for the fast emission) and no fast non-radiative channels (to enable the slow radiative channel). Thus, our experimental conditions and the chosen categorization of QDs validate the simplified approach proposed in eqn (3). Potential studies of the switching of QDs between the individual types of emission would require more detailed models and dedicated experiments.

3.4 Short-lived component and quantum yield

The determination of the fast-to-slow ratio presented in Section 3.2 lets us rewrite eqn (3), because $FTS = \frac{n^{fast}\eta_{fast}}{n^{slow}\eta_{slow}}$. The rewritten formula reads

$$\eta_E \approx \frac{1 + FTS}{\frac{1}{\eta_{slow}}\left(1 + \frac{n^{dark}}{n^{slow}}\right) + FTS\frac{1}{\eta_{fast}}}.$$

The typical internal quantum yield of the long-lived component η_{slow} can often be determined and can even be equal to one.[38] FTS, on the other hand, varies in the range of 0.003–0.1 as shown in Fig. 4f. The unknowns in the above formula are the ratio of the dark QDs to those emitting the long-lived PL $n^{dark/}$

n^{slow} and the internal quantum yield of the short-lived component η_{fast}. The last quantity η_{fast} would be extremely difficult to determine experimentally and, moreover, very likely also depends on the experimental conditions of the study, see Fig. 3. However, fast lifetimes connected with this emission ($\tau^{fast} \approx$ 3.5–20 ns) suggest that η_{fast} could be in the range of at least several percent. Thus, the impact of the short-lived component on the overall quantum yield is small (FTS ≪ 1), in contrast to the decisive impact of dark QDs, because $\eta_E \approx \eta^{slow}/\left(1 + \frac{n^{dark}}{n^{slow}}\right)$.[38] Moreover, quantum yields are typically measured using blue excitation (excitation wavelength 400–500 nm). As the short-lived component gets weaker under blue excitation, as shown in Fig. 3b and by Valenta et al.,[35] the direct influence of the short-lived component on the overall quantum should also be low.

Even though the influence of the short-lived component on the measured quantum yield should in theory be negligible, we observed that the short-lived component is systematically stronger relatively to the long-lived one in samples with lower quantum yields, see Fig. 4f. An analogical (anti)correlation was also suggested previously by an independent group,[8] where SiQDs with an extremely narrow size distribution were studied, confirming that this (anti)correlation is systematically present in SiQDs and that it does not arise purely from a broad distribution of sizes in the sample.

Even if this effect might seem counter-intuitive at first sight, it is a very simple consequence of the properties of the individual sub-ensembles of QDs. SiQDs in which fast non-radiative recombination is relatively more important can be thought of as those where an additional non-radiative channel was introduced. In reality, the relative importance of fast non-radiative recombination can increase for example as a result of "improper" surface passivation. Importantly, the introduction of a fast short-lived non-radiative channel to a QD with slow long-lived radiative recombination will render this QD dark, but its influence on the fast radiative channel will be only mild, as was shown in Table 2. Clearly, this selective lifetime-based quenching will manifest as lowered overall external PL quantum yield because the slow QDs are rendered dark, but it will at the same time lead to a higher FTS ratio by lowering the fraction of slowly emitting QDs. Thus, selective lifetime-based quenching, a simple direct consequence of the presence of QDs with significantly different lifetimes in a macroscopic ensemble, can very easily explain the seemingly counter-intuitive correlation of external quantum yield with fast blue PL signal.

4 Discussion

The extremely wide range of timescales from a few nanoseconds to a millisecond on which SiQDs emit PL signal is not a typical feature in other, more commonly investigated types of semiconductor QDs. This attribute in principle enables the possibility of tuning of lifetimes of SiQDs in a wide range, which comes with interesting application prospects. However, it also means that some of the works focused on the short-lived component may report seemingly conflicting results. One important thing to realize here is the order-of-magnitude difference between the PL rates ($r_{PL} = 1/\tau_{av}$) of the two components. For example, at the emission photon energy of 2.0 eV, r_{PL}^{slow} (2.0 eV) = 0.03 photons per (μs · QD) and r_{PL}^{fast} (2.0 eV) = 0.1 photons per (ns · QD), respectively, based on the measured lifetimes. This corresponds to 5 and 10^{-3} photons emitted on average in a 50 ns interval by a typical QD with short-lived and long-lived component, respectively. This stark contrast implies that the fast and slow channels are selectively detected by focusing either on the microsecond or the nanosecond PL decay, as summarized in Fig. 5b. This is particularly important for the determination of radiative lifetimes using the Purcell effect, which relies solely on the microsecond red-orange PL decays in SiQDs[54] and thus addresses only the properties of the long-lived PL channel.

The ratio of slow and fast PL components was already studied by Brown *et al.*[50] Importantly, they characterize only a small fraction of the fast PL band we study here, as shown in Fig. 4e by the green rectangle and, therefore, theirs and our interpretations are not directly comparable. Unlike in that report, our data is spectrally resolved and allows us to extract and compare the full spectral profiles of the two PL channels. Thus, our more in-depth characterization allows us to differentiate between the two radiative recombination channels put forward in Fig. 1b, namely the fast (<20 ns) direct recombination at or around the $\Gamma_{15} - \Gamma'_{25}$ transition in silicon and the slow (>100 ns) quasi-direct or possibly phonon-assisted radiative recombination from the cold electron states. In addition to providing the full picture, our spectrally resolved approach is also less prone to potential inaccuracies in data treatment.

An interesting direction of further research here is the question which of the processes from Fig. 5 and Table 2 limit the spectral tunability of the long-lived PL component. In our previous work,[38] we showed that the long-lived PL channel can be tuned in a wide range of emission photon energies. Other reports clearly suggest[11,14–20] that one important factor which limits the spectral tunability of the long-lived component is the exposure to oxygen. In principle, there are three possible mechanisms which can limit spectral tunability from the orange to the yellow/green spectral region. These three mechanisms are: (i) SiQDs become too small to behave as crystalline QDs, establishing a high-photon-energy limit for emitted PL, (ii) the ratio of fast non-radiative processes sharply rises in smaller QDs, which could possibly emit yellow/green PL, but this PL is effectively quenched, or (iii) smaller QDs, which possibly could emit yellow/green PL, have a high fraction of dark QDs. Mechanisms (ii) and (iii) are likely connected with faults in the crystalline core of the QD or in

its surface passivation. Although we cannot currently determine which of these processes are the determining factor, we believe it to be an important question for further study.

5 Conclusion

The radiative processes in SiQDs were studied in detail over a wide range of emission photon energies (1.7–3.3 eV) and timescales (10 ns–2 ms). We confirmed the presence of only two sets of radiative processes with significantly different lifetimes in SiQDs with either oxide or long-alkyl surface passivation. The short-lived PL is characterized by emission-wavelength-independent average PL lifetimes of 3.5–20 ns varying from sample to sample and highly non-single-exponential PL decay shape with dispersion factor $\beta \approx$ 0.5–0.6 if described using the stretched-exponential function. Both these components were detected in all the studied samples covering the three main fabrication techniques of SiQDs. Using sparse pulsed excitation, we found out that the fast-to-slow ratio varies between 3×10^{-3} and 0.1 depending on the sample. We introduced a model describing the impact of three sub-ensembles of SiQDs, namely slow, fast and dark, on the optical performance. The fast-to-slow ratio was observed to anti-correlate with the external, ensemble-averaged photoluminescence quantum yield, with samples with stronger short-lived PL exhibiting lower quantum yield. We attribute this observation to selective lifetime-based PL quenching, or in other words, the introduction of fast non-radiative processes, which preferentially render the slowly emitting QDs dark. Thus, we showed that the observed anti-correlation is an intrinsic property of a system made by the three markedly different sub-ensembles of QDs. Even though our study focuses solely on SiQDs, the approaches we introduce here, namely the experimental determination of the fast-to-slow PL ratio, the model describing the influence of different sub-ensembles of QDs on the optical performance of the ensemble, or the selective lifetime-based PL quenching can be readily generalized to other inhomogeneous systems, such as a sample of QDs or molecules containing impurities.

Author contributions

T. P. carried out the optical measurements, T. P. and K. K. analyzed and interpreted the acquired data, F. M., J. K., G. M. and P. C. fabricated the samples, P. C. and K. K. supervised the project, T. P. and K. K. co-wrote the manuscript. All the authors read and agreed on the text of the manuscript.

Conflicts of interest

There are no conflicts to declare.

Acknowledgements

We also acknowledge Prof. J. Valenta for making the quantum yield measurements.

References

1 M. V. Kovalenko, L. Manna, A. Cabot, Z. Hens, D. V. Talapin, C. R. Kagan, V. I. Klimov, A. L. Rogach, P. Reiss, D. J. Milliron, P. Guyot-Sionnnest, G. Konstantatos, W. J. Parak, T. Hyeon, B. A. Korgel, C. B. Murray and W. Heiss, *ACS Nano*, 2015, **9**, 1012–1057.

2 R. Mazzaro, F. Romano and P. Ceroni, *Phys. Chem. Chem. Phys.*, 2017, **19**, 26507–26526.

3 S. Milliken, A. N. Thiessen, I. T. Cheong, K. M. O'Connor, Z. Li, R. W. Hooper, C. J. T. Robidillo and J. G. C. Veinot, *Nanoscale*, 2021, **13**, 16379–16404.

4 D. Beri, *Mater. Adv.*, 2023, **4**, 3380–3398.

5 D. Yang, Z. Cui, Z. Wen, Z. Piao, H. He, X. Wei, L. Wang, S. Mei, W. Zhang and R. Guo, *ACS Mater. Lett.*, 2023, **5**, 985–1008.

6 K.-i. Saitow, *Bull. Chem. Soc. Jpn.*, 2024, **97**, uoad002.

7 D. C. Hannah, J. Yang, P. Podsiadlo, M. K. Y. Chan, A. Demortiére, D. J. Gosztola, V. B. Prakapenka, G. C. Schatz, U. Kortshagen and R. D. Schaller, *Nano Lett.*, 2012, **12**, 4200–4205.

8 T. A. Pringle, K. I. Hunter, A. Brumberg, K. J. Anderson, J. A. Fagan, S. A. Thomas, R. J. Petersen, M. Sefannaser, Y. Han, S. L. Brown, D. S. Kilin, R. D. Schaller, U. R. Kortshagen, P. R. Boudjouk and E. K. Hobbie, *ACS Nano*, 2020, **14**, 3858–3867.

9 L. Canham, *Faraday Discuss.*, 2020, **222**, 10–81.

10 Y. Yu, G. Fan, A. Fermi, R. Mazzaro, V. Morandi, P. Ceroni, D.-M. Smilgies and B. A. Korgel, *J. Phys. Chem. C*, 2017, **121**, 23240–23248.

11 K. Dohnalová, L. Ondič, K. Kůsová, I. Pelant, J. L. Rehspringer and R.-R. Mafouana, *J. Appl. Phys.*, 2010, **107**, 053102.

12 M. Dasog, Z. Yang, S. Regli, T. M. Atkins, A. Faramus, M. P. Singh, E. Muthuswamy, S. M. Kauzlarich, R. D. Tilley and J. G. C. Veinot, *ACS Nano*, 2013, **7**, 2676–2685.

13 K. K. Chen, M. L. Mastronardi, C. Kübel and G. A. Ozin, *Part. Part. Syst. Charact.*, 2015, **32**, 301–306.

14 P. R. Coxon, Q. Wang and Y. Chao, *J. Phys. D: Appl. Phys.*, 2011, **44**, 495301.

15 W. J. I. DeBenedetti, S.-K. Chiu, C. M. Radlinger, R. J. Ellison, B. A. Manhat, J. Z. Zhang, J. Shi and A. M. Goforth, *J. Phys. Chem. C*, 2015, **119**, 9595–9608.

16 J. R. Rodriguez Nunez, J. a. Kelly, E. J. Henderson, J. G. C. Veinot, J. R. Rodríguez Núñez, J. a. Kelly, E. J. Henderson and J. G. C. Veinot, *Chem. Mater.*, 2012, **24**, 346–352.

17 J. Choi, N. S. Wang and V. Reipa, *Langmuir*, 2007, **23**, 3388–3394.

18 Z. Kang, Y. Liu, C. H. A. Tsang, D. D. D. Ma, X. Fan, N.-B. Wong and S.-T. Lee, *Adv. Mater.*, 2009, **21**, 661–664.

19 F. Hua, M. T. Swihart and E. Ruckenstein, *Langmuir*, 2005, **21**, 6054–6062.

20 K. Dohnalová, K. Kůsová and I. Pelant, *Appl. Phys. Lett.*, 2009, **94**, 211903.

21 M. Dasog, G. B. D. los Reyes, L. V. Titova, F. A. Hegmann and J. G. C. Veinot, *ACS Nano*, 2014, **8**, 9636–9648.

22 G. M. Carroll, R. Limpens and N. R. Neale, *Nano Lett.*, 2018, **18**, 3118–3124.

23 Q. Li, Y. He, J. Chang, L. Wang, H. Chen, Y.-W. Tan, H. Wang and Z. Shao, *J. Am. Chem. Soc.*, 2013, **135**, 14924–14927.

24 K. Kůsová, P. Hapala, J. Valenta, P. Jelínek, O. Cibulka, L. Ondič and I. Pelant, *Adv. Mater. Interfaces*, 2014, **1**, 1300042.

25 A. N. Poddubny and K. Dohnalová, *Phys. Rev. B: Condens. Matter Mater. Phys.*, 2014, **90**, 245439.

26 B. van Dam, C. I. Osorio, M. A. Hink, R. Muller, A. F. Koenderink and K. Dohnalova, *ACS Photonics*, 2018, **5**, 2129–2136.

27 K. Dohnalová, P. Hapala, K. Kůsová and I. Infante, *Chem. Mater.*, 2020, **32**, 6326–6337.

28 J. B. Essner, J. A. Kist, L. Polo-Parada and G. A. Baker, *Chem. Mater.*, 2018, **30**, 1878–1887.

29 B. V. Oliinyk, D. Korytko, V. Lysenko and S. Alekseev, *Chem. Mater.*, 2019, **31**, 7167–7172.

30 J. L. Z. Ddungu, S. Silvestrini, A. Tassoni and L. De Cola, *Faraday Discuss.*, 2020, **222**, 350–361.

31 J. Wilbrink, C.-C. Huang, K. Dohnalova and J. M. J. Paulusse, *Faraday Discuss.*, 2020, **222**, 149–165.

32 G. Morselli, F. Romano and P. Ceroni, *Faraday Discuss.*, 2020, **222**, 108–121.

33 P. Galář, T. Popelář, J. Khun, I. Matulková, I. Němec, K. Newell, A. Michalcová, V. Scholtz and K. Kůsová, *Faraday Discuss.*, 2020, **222**, 240–257.

34 L. Tsybeskov, J. V. Vandyshev and P. M. Fauchet, *Phys. Rev. B: Condens. Matter Mater. Phys.*, 1994, **49**, 7821–7824.

35 J. Valenta, A. Fučíková, I. Pelant, K. Kůsová, K. Dohnalová, A. Aleknavičius, O. Cibulka, A. Fojtík and G. Kada, *New J. Phys.*, 2008, **10**, 073022.

36 W. D. A. M. de Boer, D. Timmerman, K. Dohnalova, I. N. Yassievich, H. Zhang, W. J. Buma and T. Gregorkiewicz, *Nat. Nanotechnol.*, 2010, **5**, 878–884.

37 L. Ondič, K. Kůsová, M. Ziegler, L. Fekete, V. Gärtnerová, V. Cháb, V. Holý, O. Cibulka, K. Herynková, M. Gallart, P. Gilliot, B. Hönerlage and I. Pelant, *Nanoscale*, 2014, **6**, 3837–3845.

38 T. Popelář, P. Galář, F. Matějka, G. Morsellli, P. Ceroni and K. Kůsová, *J. Phys. Chem. C*, 2023, **127**, 20426–20437.

39 R. Mazzaro, A. Gradone, S. Angeloni, G. Morselli, P. G. Cozzi, F. Romano, A. Vomiero and P. Ceroni, *ACS Photonics*, 2019, **6**, 2303–2311.

40 V. Zajac, H. Němec, C. Kadlec, K. Kůsová, I. Pelant and P. Kužel, *New J. Phys.*, 2014, **16**, 093013.

41 K. Kůsová and T. Popelář, *J. Appl. Phys.*, 2019, **125**, 193103.

42 Y. Wang and P. Townsend, *J. Lumin.*, 2013, **142**, 202–211.

43 J. Valenta, *Nanosci. Methods*, 2014, **3**, 11–27.

44 P. Hapala, K. Kůsová, I. Pelant and P. Jelínek, *Phys. Rev. B: Condens. Matter Mater. Phys.*, 2013, **87**, 195420.

45 D. Kovalev, H. Heckler, M. Ben-Chorin, G. Polisski, M. Schwartzkopff and F. Koch, *Phys. Rev. Lett.*, 1998, **81**, 2803–2806.

46 I. Sychugov, J. Valenta, K. Mitsuishi, M. Fujii and J. Linnros, *Phys. Rev. B: Condens. Matter Mater. Phys.*, 2011, **84**, 125326.

47 A. S. Moskalenko, J. Berakdar, A. N. Poddubny, A. A. Prokofiev, I. N. Yassievich and S. V. Goupalov, *Phys. Rev. B: Condens. Matter Mater. Phys.*, 2012, **85**, 085432.

48 A. A. Prokofiev, A. S. Moskalenko, I. N. Yassievich, W. D. A. M. de Boer, D. Timmerman, H. Zhang, W. J. Buma and T. Gregorkiewicz, *JETP Lett.*, 2009, **90**, 758–762.

49 Y. Kanemitsu, T. Futagi, T. Matsumoto and H. Mimura, *Phys. Rev. B: Condens. Matter Mater. Phys.*, 1994, **49**, 14732–14735.

50 S. L. Brown, J. B. Miller, R. J. Anthony, U. R. Kortshagen, A. Kryjevski and E. K. Hobbie, *ACS Nano*, 2017, **11**, 1597–1603.

51 M. Greben, P. Khoroshyy, S. Gutsch, D. Hiller, M. Zacharias and J. Valenta, *Beilstein J. Nanotechnol.*, 2017, **8**, 2315–2323.

52 D. Kovalev, J. Diener, H. Heckler, G. Polisski, N. Künzner and F. Koch, *Phys. Rev. B: Condens. Matter Mater. Phys.*, 2000, **61**, 4485–4487.

53 X. Liu, Y. Zhang, T. Yu, X. Qiao, R. Gresback, X. Pi and D. Yang, *Part. Part. Syst. Charact.*, 2016, **33**, 44–52.

54 S. Miura, T. Nakamura, M. Fujii, M. Inui and S. Hayashi, *Phys. Rev. B: Condens. Matter Mater. Phys.*, 2006, **73**, 245333.